CFD Modeling of Mass Transfer and Stripping Efficiency in FCCU Strippers

Jinsen Gao, Jian Chang, and Xingying Lan
State Key Laboratory of Heavy Oil Processing, China University of Petroleum, Beijing 102249, People's Republic of China

Yong Yang
PetroChina Planning and Engineering Institute; Beijing 100083, People's Republic of China

Chunxi Lu and Chunming Xu
State Key Laboratory of Heavy Oil Processing, China University of Petroleum, Beijing 102249, People's Republic of China

DOI 10.1002/aic.11444
Published online March 26, 2008 in Wiley InterScience (www.interscience.wiley.com).

This article presents an experimental and computational study of mass transfer characteristics and stripping efficiency of bubbling fluidized beds within FCCU strippers. The hydrodynamic and mass transfer characteristics are investigated experimentally. Based on the granular kinetics theory, a two-fluid CFD model coupled with a modified Gidaspow drag model and an empirical mass transfer model has been developed and verified against the experimental results. The overall trend of the time-averaged bed density, concentration of tracer and stripping efficiency at various superficial gas velocities were in reasonable agreement with the experimental data. It was found that stripping efficiency depends strongly on the operating conditions as well as on the internal configuration of the strippers. Increasing superficial gas velocity increases stripping efficiency. Internal baffles improve break-up and redistribution of bubbles and enhance the gas-solids contacting remarkably, showing a benefit for the mass transfer in the V-baffled stripper.
 AIChE J, 54: 1164–1177, 2008
Keywords: fluidization, FCCU stripper, stripping efficiency, Eulerian simulation, FCC catalysts

Introduction

Fluid catalytic cracking (FCC) is the main heavy oil conversion process in most petroleum refineries.[1] Circulating fluidized bed technology is used in modern FCC units where cracking reactions take place as the vaporized gas oil feed and catalyst flow up the riser. Having been disengaged from the product gas, the catalyst needs to be regenerated because of deactivation due to coke deposition. However, hydrocarbon products are entrained, adsorbed, or present on the spent catalyst. It is important to strip these hydrocarbons off quickly and efficiently prior to regeneration. Incomplete stripping leads to loss of valuable product due to their combustion in the regenerator. The increase in hydrocarbon burned also increases the regenerator temperature, and subsequently, affects the FCC unit heat balance, while promoting faster catalyst degradation and mechanical wear of components.[2,3]

Stripping is generally accomplished in a bubbling or turbulent fluidized bed by adding steam which bubbles upwards, counter-currently to the down flowing catalyst particles.[4] Understanding the hydrodynamics, mass and heat transfer in the stripper is essential for improving its performance and optimizing the design process. However, research on the stripper published in the open literature has been scarce until recently. Senior et al.[5] have described in detail the flow prob-

Correspondence concerning this article should be addressed to Chunming Xu at xcm@cup.edu.cn.

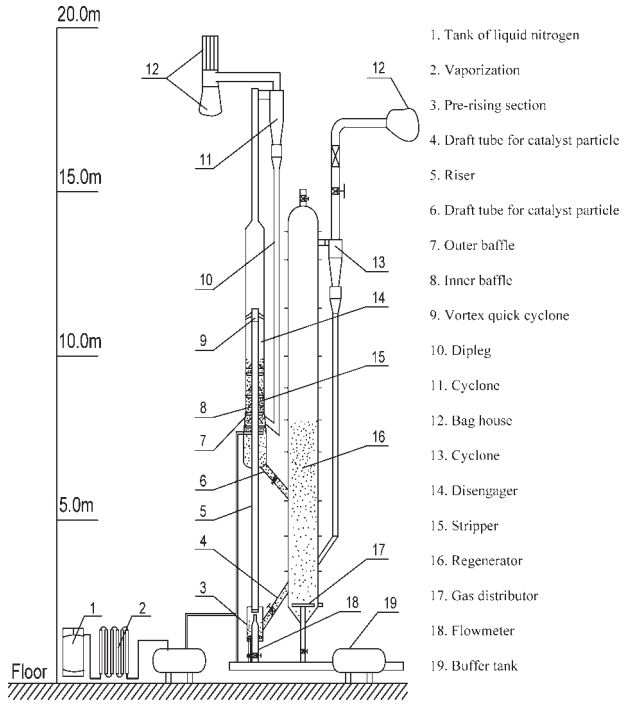

Figure 1. A schematic experimental set-up of V-baffled stripper.

lems encountered in commercial FCCU stripper operation. Cui et al.[6,7] investigated experimentally the gas–solids mixing and the effect of jet configuration on fluidized bed stripping in a dynamically scaled fluid coker stripper.

With the increase of computational power, Computational Fluid Dynamics (CFD) offers a new approach to understand the hydrodynamics and transfer mechanisms in multiphase flows. McKeen and Pugsley[8] modeled the hydrodynamics of a cold flow, laboratory scale FCCU stripper using CFD. The model successfully predicted the improved break-up and redistribution of bubbles within a baffled stripper as compared to the nonbaffled case. Furthermore, the model was successful in predicting the onset of flooding in the baffled stripper. Such calculations provided detailed information on the transient gas-solids flow behavior in the FCCU stripper. Most of the previous research in the dense gas–solids fluidized beds was limited to hydrodynamic characteristics such as two-phase flow behavior, profiles of pressure gradient, solids concentration, and velocity distributions. The gas–solids mass transfer behavior in the FCCU stripper was seldom reported. For investigating the stripping efficiency of the FCCU strippers, the previous computational study needs to be extended to include mass transfer.

The present work was undertaken to study mass transfer and stripping efficiency in the FCCU strippers. Experiments were carried out to measure the concentration profile of tracer in two FCCU strippers of different type (empty cylinder stripper and V-baffled stripper) at various operating conditions. The stripping efficiency was determined experimentally. Next, an empirical mass transfer model proposed by Miyauchi-Masao[9] was employed to investigate the interphase mass transfer in FCCU strippers. By incorporating it into the two-fluid model, an Eulerian-Eulerian CFD model for a bubbling gas-solids fluidized bed containing Geldart A particles was established to investigate the mass transfer behavior within FCCU strippers. The predicted results, such as profile of bed density, concentration of tracer and stripping efficiency at different superficial gas velocities, were evaluated and compared to experimental data. Furthermore, the effects of internal baffles on the mass transfer and stripping efficiency were investigated.

Experimental

The stripping efficiencies are systematically studied in two different types of FCCU strippers (empty cylinder stripper and V-baffled stripper). Figures 1 and 2 present a schematic experimental set-up and a detailed structure of V-baffled stripper, respectively. In Figure 2, the stripper is a cylindrical geometry with the riser located at the centerline. The annular region is the stripping space and the simulated domain. 2D cylindrical coordinates are used in the following numerical simulation since this is an annular geometry. In addition, these two strippers are composed of two stage structures. The size of the down cone is Φ600 mm × Φ486 mm× 500 mm, and size of the upper cylinder is Φ486 mm × 1500 mm. The V-baffled stripper has four pairs of V-baffles, angled at 45°. Each baffle blocks 50% of the cross-sectional flow area. The empty cylinder stripper is the same as the V-baffled stripper except that the baffles are removed.

The unit was first operated without solids circulation. At time zero, a certain amount of FCC catalyst was put in the

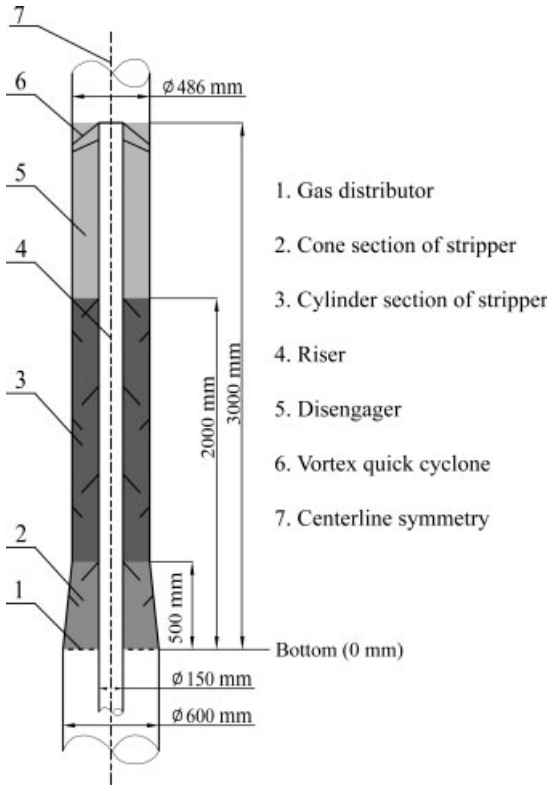

Figure 2. A detailed structure of V-baffled stripper.

Table 1. Experiment Conditions

Items	Value
Density of nitrogen	1.138 kg/m^3
Density of oxygen	1.299 kg/m^3
Diameter of FCC catalyst	58 μm
Density of FCC catalyst	1500 kg/m^3
Superficial gas velocity	0.05, 0.1, 0.15, 0.2 m/s
Catalyst inventory	230 kg
Solid mass flux	26.73 kg/(m^2·s)

stripper, and the bed height of catalyst particle was about 2.0 m. Pure nitrogen was injected through gas distributor located at the bottom of the cone section to fluidize the particles. After several seconds, steady fluidization was established. Then, solids circulation was initiated. Catalyst particles were carried upwards through the riser by air. Separated by a vortex quick separator, the catalyst particles with entrained air were introduced into the disengager and then the stripper sections. With the unit operating at steady state, the net flow of particles is downward through the stripper. Solids leave the stripper through the outlet of particles, while the gas exits from the outlet at the top of the unit.

Pressure profiles along the stripper were measured by the U-tube water manometer together with pressure transducers. Subsequently, the mean bed density can be calculated from Eq. 1.

$$\rho_b = \frac{\Delta p}{g \Delta h} \tag{1}$$

Oxygen in the air entrained by FCC particles was used to simulate feed hydrocarbon gas introduced into the stripper section. The oxygen tracer was carried continuously by catalyst particles at a constant flow rate. A series of sampling tube were employed to draw the gas simultaneous from different location of the bed. There were four sampling heights located at 500, 800, 1200, and 1800 mm above the gas distributor at the bottom of the stripper section (see Figure 2). The O_2 concentration in the stripper was determined by the TCD within a gas chromatography. Thereby, an estimate of stripping efficiency was determined based on the concentration of oxygen detected at the sampling position.

FCC particles of mean diameter of 58 μm and density of 1500 kg/m^3 were used in the experiments. The solid flux in the stripper is 26.73 kg/ (m^2 s) and the superficial gas velocity is in the range of 0.05–0.20 m/s. A summary of the material property and experimental operating conditions is found in Table 1.

CFD Model

Because of the high particle concentrations in gas-solids bubbling fluidized beds the particle–particle interactions can not be neglected. Moreover, the solid phase has properties similar to a continuous fluid. By using the kinetic theory of granular flows[10,11] the viscous forces and the solid pressure of the particle phase can be described as a function of the so-called granular temperature. Therefore, the Eulerian model using kinetic theory for granular flow was shown to be suitable for modeling dense gas-solids fluidized bed reactors. This leads to the following differential equations given in the Eulerian notation. The conservation and constitutive equations are provided in the Appendix. Inter-phase momentum exchange coefficient (β) and inter-phase mass transfer rate (m_{gsps}) are described in detail in the next two sections, respectively.

Gas-solids drag for bubbling fluidized bed of FCC catalysts

Many researchers have successfully performed bubbling fluidized bed simulations of the more coarse Geldart B particles with various model validation.[12–15] However, there have been seldom successful simulations reported up to date in the literature on bubbling beds of fine Geldart A particles. Calculations always gave a severe overestimation of the experimentally observed bed expansion. McKeen[8] pointed out that the generally poor simulation results for Geldart A particles can be attributed to the existence of significant inter-particle forces that are neglected in most simulations. The existence of cohesive inter-particle forces leads to grouping of particles, resulting in larger effective particle sizes and hence reduced fluid-particle drag forces, yielding a reduced bed expansion.

In general, the superficial gas velocity should be lower than the terminal settling velocity of a single particle in order to maintain steady fluidization. Whereas, for the fluidized bed of FCC catalysts, fluidization remains steady at gas velocities greater than the terminal setting velocity of a single particle. This phenomenon might be due to the cohesive inter-particle forces due to the Van der Waals attraction, which are responsible for agglomeration of particles and lead to a reduced drag force for FCC particles.

Lettieri et al.[16] found that, for the FCC catalyst in the fluidized bed, the experimentally obtained terminal velocity (u_t^*) is much higher than the calculated one (u_t). If the homogeneous bed was assumed to be characterized by the presence of clusters, the diameter of clusters, d_p^*, can be back-calculated from the experimental u_t^* values. Lettieri et al.[16] also calculated effective particle diameters in the range of 200–474 μm for FCC catalysts with Sauter mean diameters from 49 to 71 μm. Based on the results above, an effective mean diameter of 265 μm (the diameter of particle clusters) is determined instead of the actual 58 μm FCC particle to modify the Gidaspow drag force model in this article. This modification combines the influence of inter-particle forces, and hence the effect of particle agglomeration on the drag force. This drag force model gives reasonable hydrodynamic predictions in comparison to experimental bed expansion data in the FCCU stripper, and can be expressed as follows.

For $\alpha_g > 0.8$, β is calculated by

$$\beta = \frac{3}{4} C_D \frac{\alpha_p \alpha_g \rho_g \left|\vec{u}_p - \vec{u}_g\right|}{d_p^*} \alpha_g^{-2.65} \tag{2}$$

For $\alpha_g \leq 0.8$, β is calculated with the Ergun equation as

$$\beta = 150 \frac{\alpha_p (1-\alpha_g) \mu_g}{\alpha_g (d_p^*)^2} + 1.75 \frac{\rho_g \alpha_p \left|\vec{u}_p - \vec{u}_g\right|}{d_p^*} \tag{3}$$

where,

$$C_D = \begin{cases} \frac{24}{Re_p}\left(1 + 0.15Re_p^{0.687}\right) & \left(Re_p \le 1000\right) \\ 0.44 & \left(Re_p > 1000\right) \end{cases} \quad (4)$$

$$Re_p = \frac{\alpha_g \rho_g d_p^* \left|\vec{u}_g - \vec{u}_p\right|}{\mu_g} \quad (5)$$

Inter-phase mass transfer model

In the FCCU stripper, the concentration distribution of hydrocarbon and the stripping efficiency depend strongly on the gas-solids mass transfer. So, studies on the characteristics of inter-phase mass transfer are essential for its design and development.

In literature, two kinds of models are employed to estimate the gas–solids mass transfer behavior. One originates from the analogies between convective heat transfer and mass transfer in the fluidized bed. This expression is given in terms of the Sherwood number, from which the gas–solids mass transfer coefficient (k_g) can be estimated.[17,18] The mass transfer interfacial area (a_i), however, needs to be determined by additional experiments in the fluidized bed.

For the other type of model, the empirical correlations are derived from fluidization experiments. Numerous correlations for determining inter-phase mass transfer have been developed for bubbling beds or turbulent beds.[9,19–21] In these models, the inter-phase mass transfer efficiency in the fluidized bed is usually expressed by a volumetric mass transfer coefficient ($k_g a_i$). Miyauchi-Masao[9] presented an empirical correlation to predict the volumetric mass transfer coefficient in bubbling and turbulent beds of FCC catalyst for a superficial gas velocity range of 0.1–0.5 m/s, which was expressed as

$$k_g a_i = 25.2 U_0^{0.75} \alpha_g \quad (6)$$

where, k_g is the mass transfer coefficient, and a_i is the mass transfer interfacial area per unit volumetric bed. This mass transfer model proposed by Miyauchi-Masao is used in the present work, which is expected to give reasonable mass transfer rate predictions in FCCU stripper. Therefore, the mass transfer rate (m_{gsps}) between the gas phase and particle phase can write as

$$m_{gsps} = k_g a_i \left(\alpha_g \rho_g Y_{gs} - \alpha_p \rho_p Y_{ps}\right) \quad (7)$$

where, m_{gsps} is the inter-phase mass transfer rate of species s.

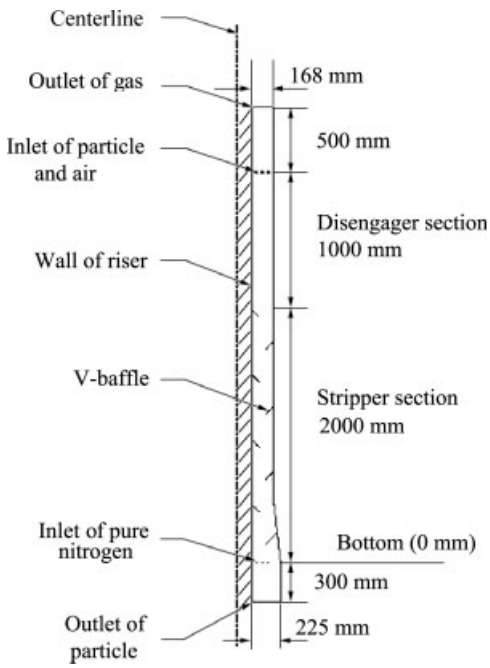

Figure 3. Detailed structure of V-baffled stripper used in the simulation.

Table 2. Simulation Parameters Used in Fluent 6.2.16

Flow type	Laminar
Gas-solid model	Eulerian-Eulerian, with kinetic theory
Drag model	Modified Gidaspow
Solids Pressure	Lun et al.[25]
Granular viscosity	Gidaspow[11]
Granular bulk viscosity	Lun et al.[25]
Granular temperature	Gidaspow[11]
Granular dissipation	Lun et al.[25]
Radial distribution function	Ding and Gidaspow[12]
Wall boundary condition	No slip
Time step used	1×10^{-4} s
Max. number of iterations per time step	20
Convergence criteria	10^{-3}
Pressure velocity coupling	SIMPLE
Under-relaxation factors	0.3 for pressure, 0.5 for momentum and 0.2 for volume and granular temperature
Maximum solid packing volume fraction	0.6
Discretization scheme	First-order upwind
Restitution coefficient (e)	0.95
Outlet condition	Atmosphere pressure
Air density	1.225 kg/m^3
Air viscosity	1.7894×10^{-5} kg/(m s)
Nitrogen density	1.138 kg/m^3
Nitrogen viscosity	1.667×10^{-5} kg/(m s)
FCC particle density	1500 kg/m^3

Simulation code and numerical algorithm

Simulations were conducted using a commercial CFD soft package, Fluent 6.2.16, with the Eulerian model using kinetic theory for granular flow. In the Fluent computer program that was used in this study, the governing equations were discretized using the control volume method. The whole calculation domain is divided into a finite number of control volumes. The conservation equations are integrated in the space and time. This integration is performed using upwind differencing scheme in space and time. Either a first-order upwind

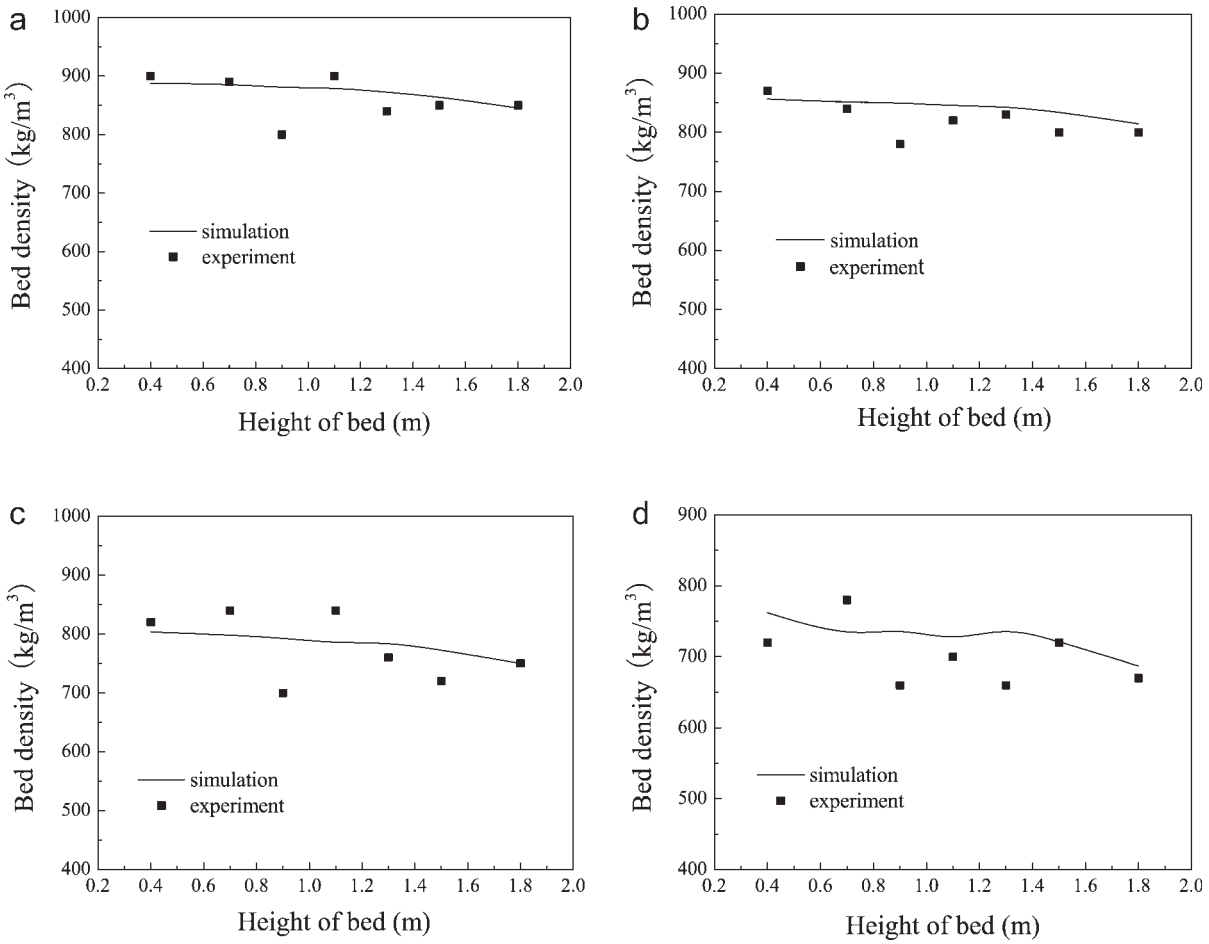

Figure 4. Axial bed density profile in the empty cylinder stripper for various superficial gas velocities.

(a) (U_0 = 0.05 m/s); (b) (U_0 = 0.10 m/s); (c) (U_0 = 0.15 m/s); (d) (U_0 = 0.20 m/s).

or a second-order discretization may be selected in Fluent 6.2.16. Although the first-order discretization generally yields less accurate results than the second-order scheme, it generally will yield better convergence. Moreover, for a simple flow that is aligned with the grid, the numerical diffusion will be low, so we use the first-order scheme instead of the second-order scheme without significant loss of accuracy.[22]

The sets of governing equations discretized are solved sequentially. The solution of the pressure profile from the gas phase momentum balance requires a pressure correction equation that corrects the pressure and velocities after each iteration of the discretized momentum equations. In this work, the popular SIMPLE algorithm by Patankar[23] is used for this purpose.

A total simulation time much greater than the mean gas residence time is selected to ensure that the simulation duration is long enough to establish the desired operating conditions. The time-averaged distributions of variables are computed covering a period of the last 5 s.

Model geometry, boundary, and initial conditions

The simulations of stripping efficiency are carried out on two experimental FCCU strippers mentioned in the previous section. The detailed structure of the V-baffled stripper used in the simulation is shown in Figure 3.

2D cylindrical coordinates are used since this is an annular geometry. The annular region is simulated by specifying a

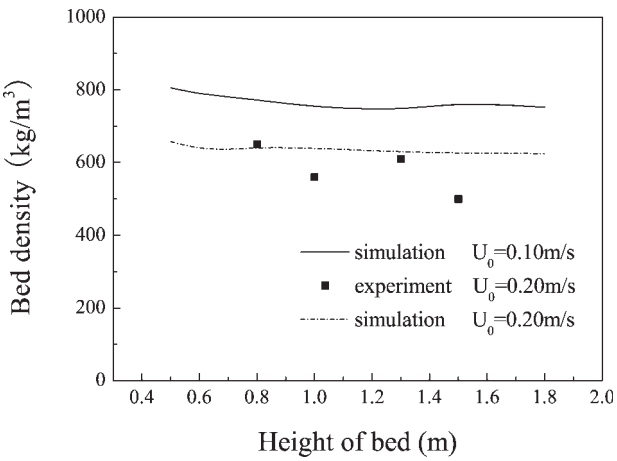

Figure 5. Effect of gas velocity on the bed density profile in the axis direction.

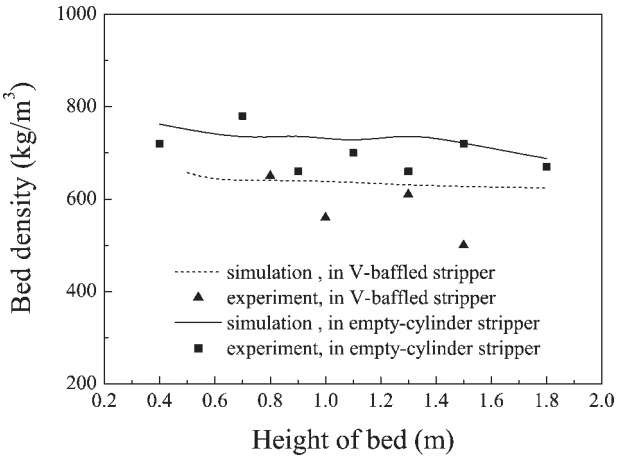

Figure 6. Comparison of axis bed density profile in the empty-cylinder stripper with that in the V-baffled stripper (U_0 = 0.2 m/s).

"dummy riser" at the centerline. Grids are created with CAD program GAMBIT 2.2.30 and exported into Fluent 6.2.16. The grid size of 0.005 m × 0.005 m is equidistant in both the horizontal and vertical directions in both strippers. This grid size is found to be an optimum between computational effort and numerical diffusion. Additionally, the grid is divided into a lower zone and an upper zone for the purpose of specifying initial conditions.

Inlet of pure nitrogen, Inlet and Outlet of particle carrying air are designated as Velocity Inlet boundary conditions in Fluent software, where the direction of gas or particle flow is normal to the surface. Flow rates used for each Velocity Inlet are determined from the superficial velocity required to match the experiments.

The outlet of gas at the top of the bed is set as Pressure Outlet boundary condition. The outlet boundary condition was a specified constant pressure (atmospheric); solids are free to leave if entrained, and are not returned to the computational domain. Everywhere else are boundary conditions specified as Wall, which are all set as no-slip wall boundary condition for both gas and particle phase. It seems not very important what kind of slip condition is chosen at the wall, as long as particles are able to fall down at the wall.[24]

At time zero, the upper zone contains no solids, while the lower zone is filled with solids at an appropriate volume fraction. The initial concentration of solid phase is based upon the maximum packing fraction for the material (0.60). The initial

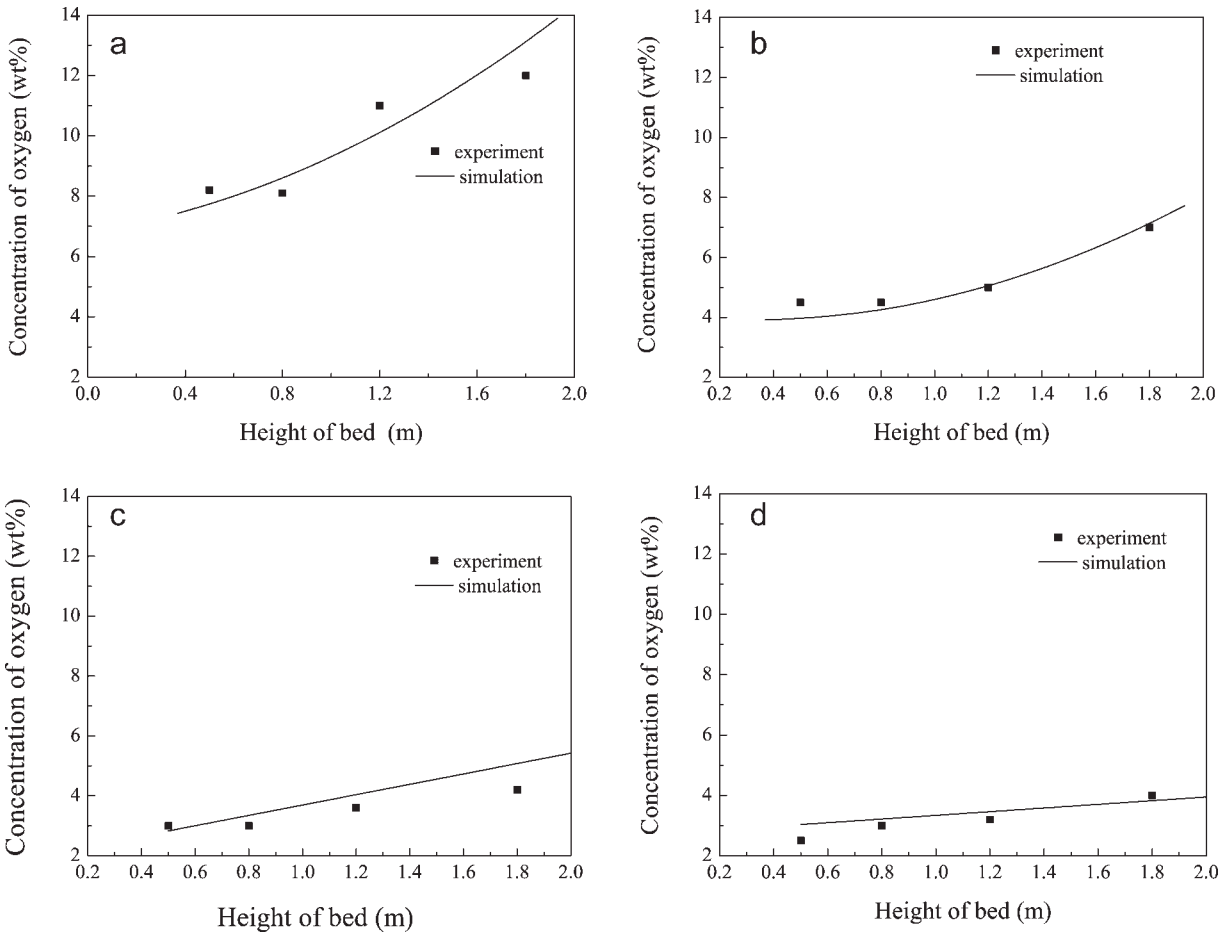

Figure 7. Axial distribution profile of oxygen concentration in the empty cylinder stripper for various superficial gas velocities.

(a) (U_0 = 0.05 m/s); (b) (U_0 = 0.10 m/s); (c) (U_0 = 0.15 m/s); (d) (U_0 = 0.20 m/s).

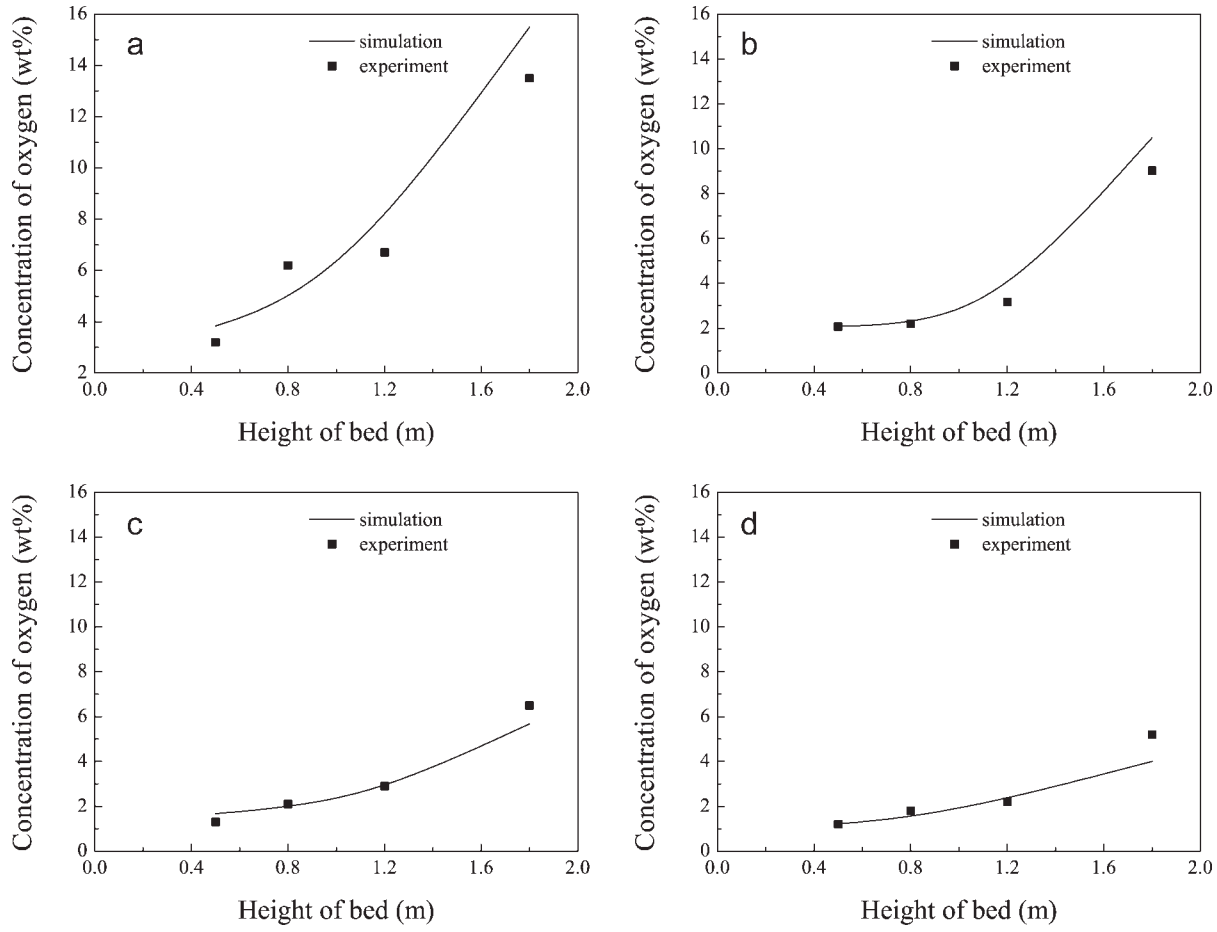

Figure 8. Axial distribution profile of oxygen concentration in V-baffle stripper for various superficial gas velocities.

(a) (U_0 = 0.05 m/s); (b) (U_0 = 0.10 m/s); (c) (U_0 = 0.15 m/s); (d) (U_0 = 0.20 m/s).

velocity of the solid phase was set to be zero. Table 2 summarizes the numerical parameters for the simulations.

Results and Discussion

Axial bed density profile

Axial Bed Density Profile in the Empty Cylinder Stripper. Figure 4 shows the comparison of bed density profile in the axial direction between simulated and experimental results for different superficial gas velocities. It can be found that the predicted bed density profile in the axial direction is in reasonable agreement with experimental results, which validates the drag force model.

As shown in Figure 4, bed density decreases slightly in the axial direction of the stripper. Moreover, the bed density decreases with increasing superficial gas velocity at a fixed height of the stripper.

Bed densities are 750–900 kg/m^3 at the superficial gas velocity of 0.05–0.10 m/s, which implies that the size and number of bubbles formed at this superficial gas velocity are small. These bubbles do not perturb the bed particles drastically. Consequently, the bed expends slightly, about 10%.

When increasing the superficial gas velocity from 0.05–0.10 m/s to 0.15–0.20 m/s, a great number of bubbles are formed in the stripper. Bubbles ascend with size and velocity gradually increasing. This causes the bed to expand evidently. At gas velocities of 0.15–0.20 m/s the bed density is 650–850 kg/m^3, and the expansion ratio is 1.2–1.3. Experimental data of bed density are qualitatively in agreement with the model estimates.

Axial Bed Density Profile in the V-Baffled Stripper. The bed densities at superficial gas velocities of 0.1 and 0.2 m/s in the V-baffled stripper are illustrated in Figure 5. Similar to the nonbaffled case, bed densities decrease slightly in the axial direction. Moreover, bed densities decrease with increasing the superficial gas velocity at a fixed height of the stripper.

Relative to the empty cylinder stripper, the V-baffled stripper shows much higher gas rise velocities due to the more restricted flow area. Consequently, as shown in Figure 6, the bed densities in the V-baffled stripper are lower than those in the empty cylinder stripper.

Axial concentration profile of oxygen in the dense zone of strippers

Axial Bed Density Profile in the Empty Cylinder Stripper. Figure 7 shows the axial concentration distribution of oxygen in the empty cylinder stripper at various superficial

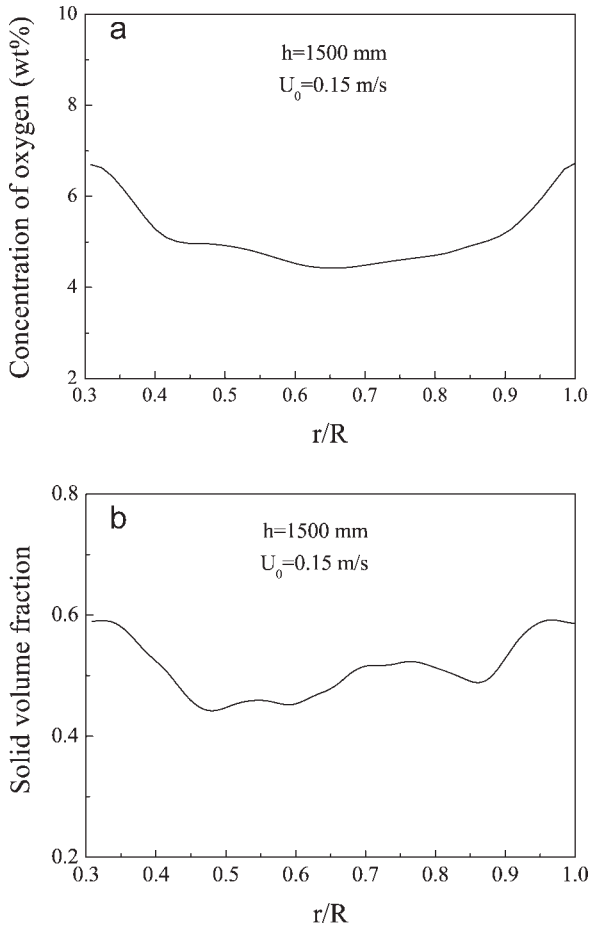

Figure 9. Radial distribution of (a) oxygen concentration; (b) solid volume fraction.

gas velocities. As shown in Figure 7, the predicted concentration profile of oxygen in the axial direction is in good agreement with experimental results, which validates the mass transfer model.

It can be found that the O_2 concentration decreases with decreasing bed height at a constant gas velocity. At the lower bed height positions, the particles entraining air stay for a relatively long time in the stripper, which results in a sufficient gas–solids contact. More oxygen is stripped by the nitrogen, resulting in a decrease in O_2 concentration.

At low gas velocities (0.05–0.10 m/s), the O_2 concentration decreases more drastically in the upper bed and then more gradually down the bed. In this case, the inter-phase mass transfer rate is not extremely high so that not all oxygen is immediately desorbed in the upper part of the bed. Therefore, the concentration driving force remains reasonably high, resulting in a decreasing concentration profile toward the bottom of the bed.

At high gas velocities (0.15–0.20 m/s), the O_2 concentrations also decrease with decreasing bed height. The decrease extent, however, is very slight toward the bottom of the bed. In the case of high gas velocity, the inter-phase mass transfer rate is relatively high throughout the bed. The oxygen concentration is reduced to very low values upon first contact with the stripping gas at the top part of the bed. Since the oxygen concentration is already low, a quasi-equilibrium situation is established, and its concentration can not be reduced much further when going downward toward the bottom of the bed.

Axial Distribution Profile of Oxygen Concentration in the V-Baffle Stripper. Figure 8 illustrates the axial concentration distributions of oxygen in the V-baffled stripper at various superficial gas velocities.

Similar to those in the empty cylinder stripper, O_2 concentration also decreases with decreasing bed height at a constant superficial gas velocity. The O_2 concentration decreases more drastically in the upper bed and then more gradually down the bed at the low superficial gas velocity. When the gas velocity is higher than 0.10 m/s, there is only a slight change in the concentration of oxygen. In addition, the O_2 concentration decreases with increasing superficial gas velocities for a fixed height of the stripper.

The O_2 concentration in the V-baffled stripper is lower than that in the nonbaffled case for the same superficial gas velocity and bed height. In the V-baffled stripper, internal baffles improved break-up and redistribution of bubbles. Bubbles split and coalesce from tray to tray over and over again and create a great number of smaller bubbles. The mass transfer interfacial area between the gas and particle phase thereby increases drastically, which is beneficial for the inter-phase mass transfer. Moreover, each baffle blocks 50% of the cross-sectional flow area in the V-baffled stripper. Because of the constrained flow area, the mass transfer is enhanced because of the higher relative velocity and the enhanced turbulence, resulting in improved nitrogen stripping and leading to reduced O_2 concentration. Therefore, the V-baffled stripper shows a lower O_2 concentration comparing to the nonbaffled case.

Radial concentration profile of oxygen in the dense zone of strippers

Radial Concentration Profile of Oxygen in the Empty Cylinder Stripper. Figure 9a shows the radial concentration

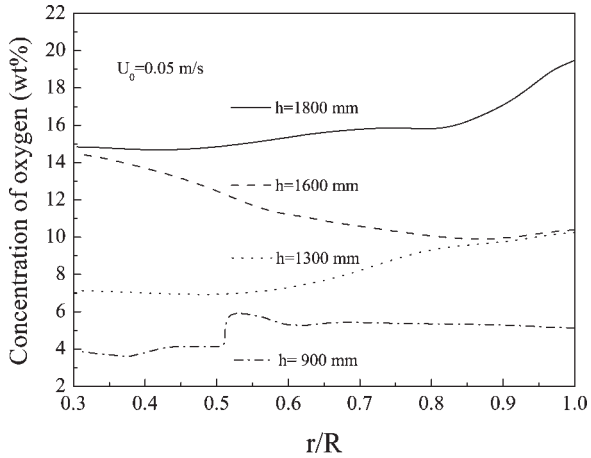

Figure 10. Radial concentration distributions of oxygen for various bed heights.

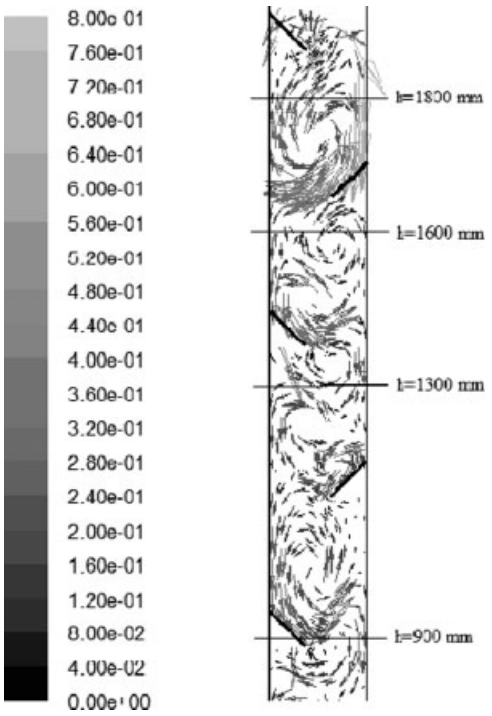

Figure 11. Local velocity vector profile of particulate phase in the V-baffled stripper.

distributions of oxygen in the empty cylinder stripper for a superficial gas velocity of 0.15 m/s and at a bed height of 1500 mm. The O_2 concentration is approximately symmetrical in the radial direction of the empty cylinder stripper, being high along the wall and low in the core region. Comparing to the axial solid volume fraction profile shown in Figure 9b, it can be found that the oxygen concentration profile is quite similar to the solid volume fraction profile: in the high solid volume fraction region, the oxygen concentration is also high and vice versa.

Radial Concentration Profile of Oxygen in the V-Baffled Stripper. The radial concentration distributions of oxygen in the V-baffled stripper are shown in Figure 10 for a superficial gas velocity of 0.05 m/s and for various bed heights. Comparing to the nonbaffled case, O_2 concentration is not uniform or symmetric in the radial direction of the V-baffled stripper. O_2 concentration is each time high on one side and low on the other side, which is closely related to the internal configuration and flow behavior.

At a height of 1800 mm, the inner baffle is located on the wall of the riser (left side of the plot, $r/R = 0.3$). Blocked by the baffle, catalyst particles containing oxygen at high concentration level tend to flow down on the right side. Thus, oxygen shows a high concentration on the right side and a low concentration on the other side. At a height of 1600 mm, the baffle is located on the outer wall (right side of the plot, $r/R = 1$). Thus, O_2 concentrations are high on the left side and low on the right side. O_2 concentration at a height of 900 mm shows a discontinuous profile on the left side of the plot, which should be attributed to the dead flow zone under the baffle. This phenomenon was also observed in the experiment, which is desired to be eliminated by some modification to the baffle. Figure 11 shows a local velocity vector profile of particulate phase within the V-baffled stripper.

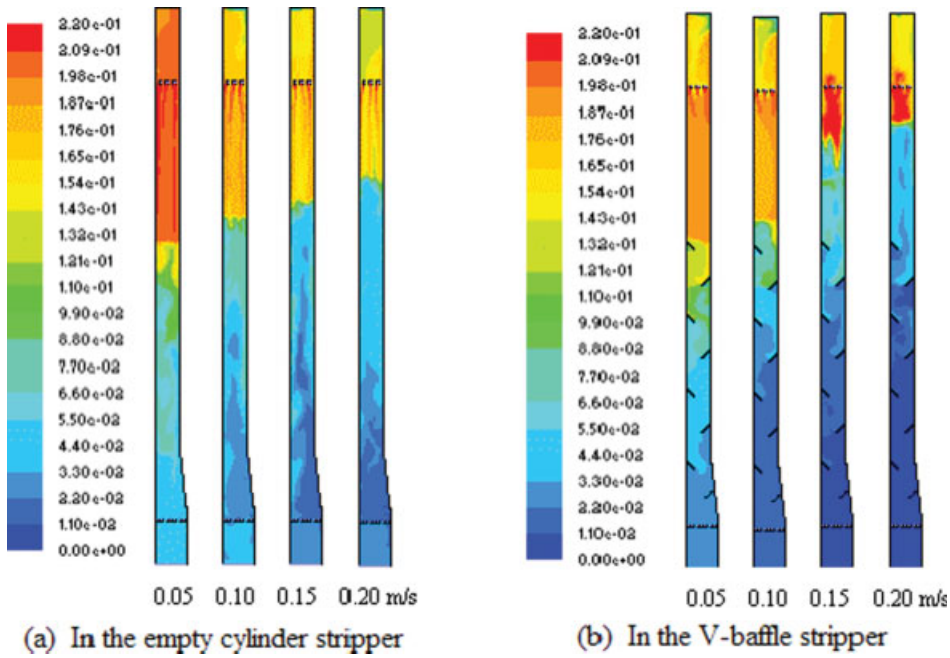

Figure 12. Transient distributions of oxygen concentration for various gas velocities.

(a) (In the empty cylinder stripper); (b) (in the V-baffle stripper).

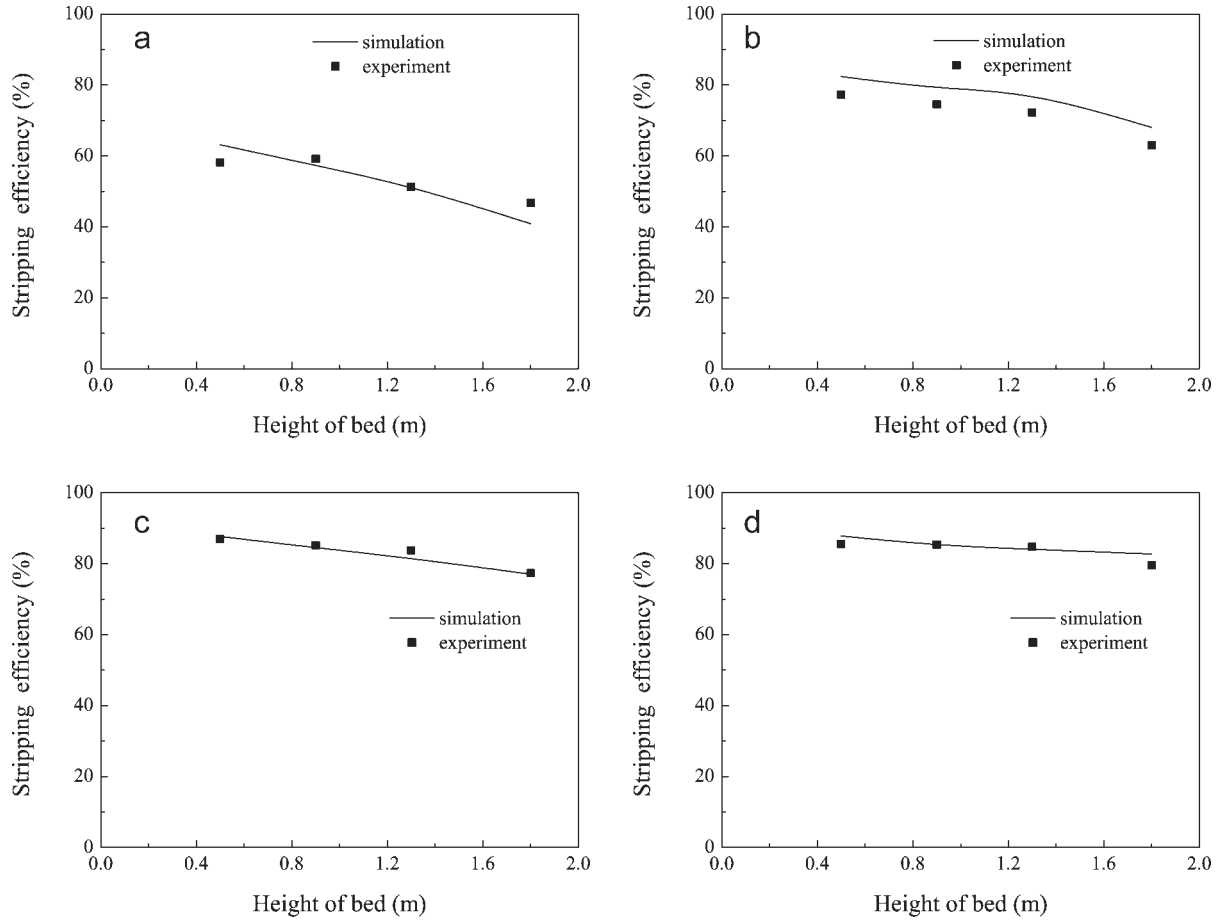

Figure 13. Comparison between predicted stripping efficiency with the measured one in the empty cylinder stripper for various superficial gas velocities.

(a) (U_0 = 0.05 m/s); (b) (U_0 = 0.10 m/s); (c) (U_0 = 0.15 m/s); (d) (U_0 = 0.20 m/s).

Transient concentration profiles of oxygen in the empty cylinder stripper and V-baffled stripper for various values of superficial gas velocities are shown in Figure 12a, b, respectively.

As shown in Figure 12, axial O_2 concentrations decrease with decreasing bed height at a constant superficial gas velocity. The O_2 concentrations also decrease with increasing superficial gas velocity for a fixed height of bed. In addition, the radial concentration profile of oxygen shows that the behavior of empty cylinder stripper deviates from that of plug flow. However, in the V-baffled stripper, the baffles clearly reduce axial solids mixing, while increasing radial mixing, as well as improving gas–solids contacting.

Stripping efficiency in both strippers

Experiment and simulation have been carried out to obtain axial tracer (oxygen) concentration profiles in the stripper. The aim was to determine how much tracer descended through the bottom outlet of the stripper, and hence to estimate the "stripper efficiency". Experiment and simulation provided the detailed distribution profile of oxygen concentration allowing the estimate of local stripping efficiencies.

Stripping efficiency is defined by

$$\eta = \frac{C_0 - C}{C_0} \times 100\% \tag{8}$$

where C_0 is the initial concentration of oxygen entrained through the top feed inlet and C is the cross-sectional-averaged concentration of oxygen at the sampling height. A local "stripping efficiency" was determined based on oxygen concentration detected across the section of each height.

At the 0 mm bottom of the strippers, the stripping agent, nitrogen, is just injected into the catalyst bed. The flow pattern and mixing is uneven and unsteady. Most components within the gas phase are nitrogen. Gas samples here cannot represent the reality of stripping efficiency. Sampling at a height of 500 mm above the bottom is representative based on the experiments. Therefore, the stripping efficiency at the height of 500 mm above the gas distributor was used to evaluate the overall stripping efficiency of the reactors.

Figures 13 and 14 show the comparison between the calculated stripping efficiencies and experimental results at vari-

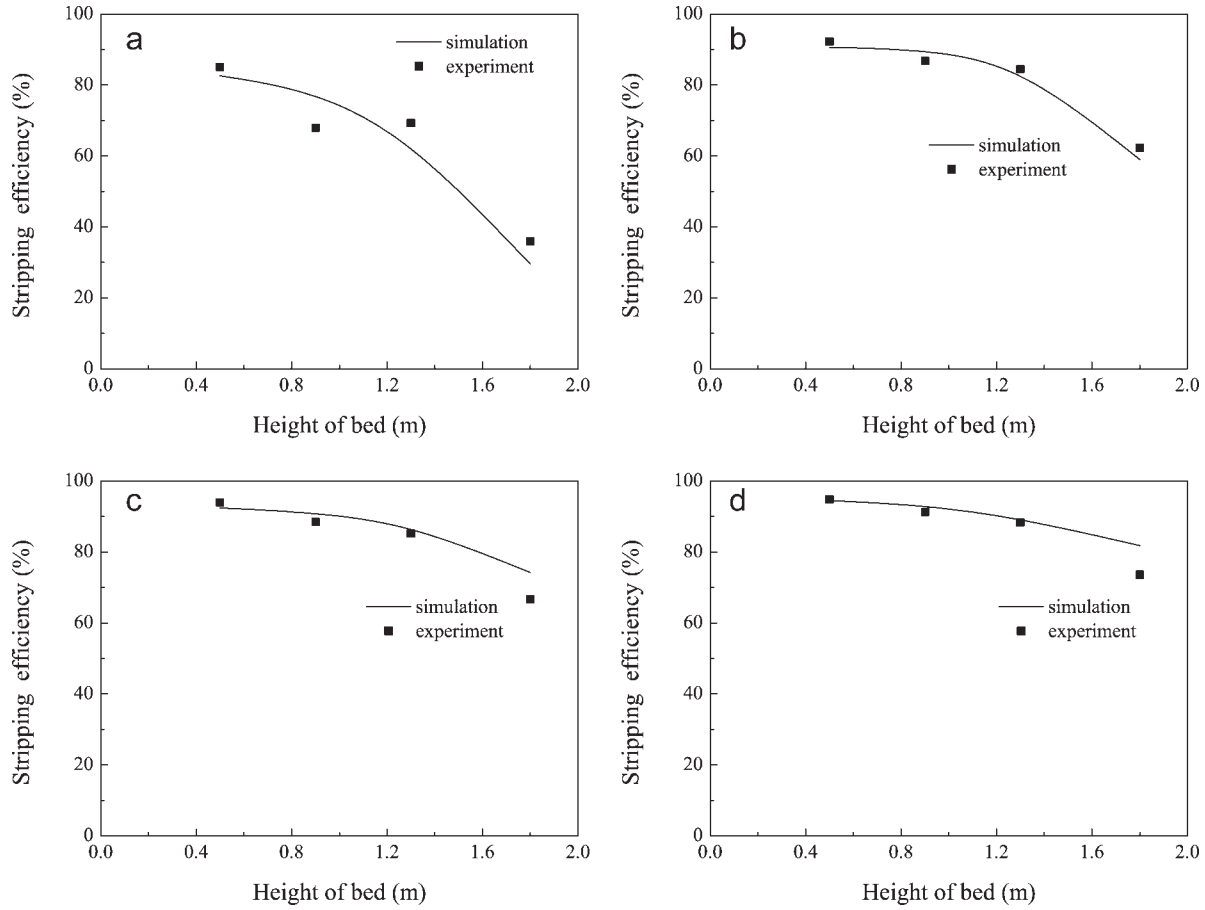

Figure 14. Comparison between predicted stripping efficiency with the measured one in the V-baffled stripper for various superficial gas velocities.

(a) (U_0 = 0.05 m/s); (b) (U_0 = 0.10 m/s); (c) (U_0 = 0.15 m/s); (d) (U_0 = 0.20 m/s).

ous superficial gas velocities in the empty cylinder stripper and V-baffled stripper, respectively. The predicted stripping efficiency in the axial direction is in good agreement with experimental results.

From Figures 13 and 14, one can see that stripping efficiencies increase with decreasing bed height for a constant superficial gas velocity in both strippers. With decreasing bed height, the particles entraining the oxygen remain for a relatively long time in the stripper, which causes sufficient gas–solids contacting and higher mass transfer efficiency. It was also found that stripping efficiency increases with superficial gas velocity for a fixed bed height in the both strippers. With increasing the gas velocity, more and more bubbles appear in the stripper frequently, which increases the mass transfer interfacial area. Moreover, increasing gas velocity also enhances the turbulent movement in the gas–solids flow. Therefore, higher stripping efficiency appears at higher gas velocity.

Table 3 compares the overall stripping efficiency in the empty cylinder stripper with that in the V-baffled stripper at various superficial gas velocities. It can be found that the V-baffled stripper shows higher overall stripping efficiencies than the empty cylinder stripper. Internal baffles improve bubble break-up and redistribution. Bubbles split and coalesce from baffle to baffle generating a great number of

Table 3. Comparison Between the Overall Stripping Efficiency in the Empty Cylinder Stripper with that in the V-Baffled Stripper

	Overall Stripping Efficiency %					
	Empty Cylinder Stripper		V-Baffled Stripper		Increment	
Superficial gas velocity m/s	Experiment	Simulation	Experiment	Simulation	Experiment	Simulation
0.05	58.2	63.2	85.1	82.6	26.9	19.5
0.10	77.3	82.3	92.3	90.6	15.0	8.3
0.15	87.0	87.7	94.0	92.4	7.0	4.7
0.20	85.5	87.8	94.8	94.5	9.3	6.7

smaller bubbles and an increased mass transfer interfacial area. Moreover, at high gas velocity V-baffle designs operate in a mode where gas rises in a turbulent annulus zig-zagging through the gaps between a baffle, which also enhances the gas–solids contacting. Thus, the V-baffled stripper show greater mass transfer rate and overall stripping efficiencies than that in the empty cylinder stripper.

Conclusions

The mass transfer and stripping efficiency in FCCU strippers were investigated systematically by using experiment and CFD method. The predicted values of the bed density, concentration distribution of oxygen and stripping efficiency are in reasonable agreement with experimental results. The absolute average relative error of the stripping efficiency is 3.2%. These validate the CFD model. The work presented here allows us to draw the following conclusions:

Bed densities decrease slightly in the axial direction in both strippers. Moreover, bed densities decrease with increasing superficial gas velocity at a fixed height of the stripper. However, compared to the empty cylinder stripper, the V-baffled stripper shows much greater gas rise velocities due to the restricted flow area. As a result, the bed density in the V-baffled stripper is lower than that in the empty cylinder stripper.

In both strippers, the axial concentration of oxygen decreases with decreasing bed height at a constant superficial gas velocity. In addition, the oxygen concentration decreases with increasing superficial gas velocities for a fixed height of the stripper. However, the V-baffled stripper shows a lower oxygen concentration relative to the nonbaffled case. The oxygen concentration is approximately symmetrical in the radial direction of the empty cylinder stripper, showing a high value along the wall and a low value in the core region. In contrast, the concentration of oxygen is high on one side and low on the other side in the V-baffled stripper.

Stripping efficiencies increase with decreasing bed height and increasing gas velocity in both strippers. Internal baffles in the V-baffled stripper improve bubble break-up and redistribution, which enhances the gas-solids contact. Thus, the V-baffled stripper shows greater mass transfer rates and overall stripping efficiencies than the empty cylinder stripper.

Experiment and simulation results showed that mass transfer and stripping efficiency in the FCCU stripper are closely related to both the internal configuration and operating conditions. They depend intrinsically on the flow behavior and gas–solids contacting in the reactor.

Acknowledgments

The authors acknowledge the supports by the National Natural Science Foundation of China through the program "Multiple Scale Analysis and Scaling-up of Direct Coupled Dual Gas-Solid Fluidized Reaction Systems" (Grant No. 20490202), the programs for Distinguished Young Scholars of China (Grant No. 20525621 and Grant No. 20725620).

Notation

a_i = mass transfer interfacial area per unit volumetric bed, $m^2\ m^{-3}$
C = concentration of oxygen at the sampling height, wt%
C_0 = initial concentration of oxygen, wt%
C_D = drag coefficient
d = diameter of particle, m
d_p^* = effective mean diameter of particle cluster, m
D = species mass diffusion coefficient, $m^2\ s^{-1}$
e = restitution coefficient
g = acceleration of gravity, $m\ s^{-2}$
g_0 = radial distribution function
h = bed height, m
k_g = mass transfer coefficient, $m\ s^{-1}$
m = inter-phase mass transfer rate, $kg\ m^{-3}\ s^{-1}$
p = pressure, Pa
r = radial direction, m
R = diameter of bed, m
Re = Reynolds number
t = time, s
u = velocity, $m\ s^{-1}$
$\vec{u}$ = velocity vector, $m\ s^{-1}$
U_0 = superficial gas velocity, $m\ s^{-1}$
u_p' = instantaneous turbulent component of velocity, $m\ s^{-1}$
u_t = terminal velocity for a single particle, $m\ s^{-1}$
u_t^* = experimental terminal velocity, $m\ s^{-1}$
x = direction coordinate
Y = specie mass fraction

Greek letters

α = volume fraction
β = inter-phase momentum exchange coefficient, $kg\ m^{-3}\ s^{-1}$
γ = collisional dissipation of energy fluctuation, $kg\ m^{-3}\ s^{-1}$
ξ = bulk viscosity, Pa s
Θ = granular temperature, $m^2\ s^{-2}$
η = stripping efficiency
μ = solid phase shear viscosity, Pa s
μ_{dil} = solid phase dilute viscosity, Pa s
ρ = density, $kg\ m^{-3}$
τ = stress tensor, Pa
Γ_Θ = diffusion coefficient for the energy fluctuation, $kg\ m^{-1}\ s^{-1}$

Subscripts

b = fluidized bed
i, j, k = direction coordinate
g = gas phase
max = maximum
p = particulate phase
s = species

Literature Cited

1. Avidan AA, Edwards M, Owen H. Innovative improvements highlight FCC's past and future. *Oil Gas J*. 1990;88:33–54.
2. McCarthy SJ, Raterman MF, Smalley CG, Sodomin JF, Miller RB. Refiner improves FCC yields using latest process technologies. *Oil Gas J*. 1997;95:56–69.
3. McKeen T, Pugsley TS. Simulation of cold flow FCC stripper hydrodynamics at small scale using computational fluid dynamics. *Int J Chem React Eng* 2003;1:A18.
4. King D. Fluidized catalytic crackers: an engineering review. In: Fluidization VII, Potter OP, Nicklin DJ, editors. *Engineering Foundation*. New York, 1992;15–26.
5. Senior RC, Smalley CG, Gbordzoe E. Hardware modifications to overcome common operating problems in FCC catalyst strippers. In: Fluidization IX, Fan LS, Knowlton TM, editors. *Engineering Foundation*. New York, 1998;725–732.
6. Cui HP, Grace JR, McKnight C, Zhang TZ, Rose I, Bi XT, Lim J, Burgardt D. Jet configuration for improved fluidized bed stripping. *Chem Eng J*. 2006;125:1–8.
7. Cui HP, Strabel M, Rusnell D, Bi XT, Mansaray K, Grace JR, Lim CJ, McKnight CA, Bulbuc D. Gas and solids mixing in a dynamically scaled fluid coker stripper. *Chem Eng Sci*. 2006;61:388–396.
8. McKeen T, Pugsley TS. Simulation and experimental validation of a freely bubbling bed of FCC catalyst. *Powder Technol*. 2003;129:139–152.

9. Miyauchi T, Masao YJ. Correction of the temperature difference between bubbles and emulsion phase and revise gas rate in fluidized beds. *J Chem Eng Jpn*. 1988;21:663.
10. Sinclair JL, Jackson R. Gas-particle flow in a vertical pipe with particle-particle interactions. *AIChE J*. 1989;35:1473–1496.
11. Gidaspow D. *Multiphase Flow and Fluidization: Continuum and Kinetic Theory Description*. Boston: Academic Press, 1994.
12. Ding J, Gidaspow D. A bubbling fluidization model using kinetic theory of granular flow. *AIChE J*. 1990;36:523–538.
13. Peirano E, Delloume V, Leckner B. Two- or three-dimensional simulations of turbulent gas-solid flows applied to fluidization. *Chem Eng Sci*. 2001;56:4787–4799.
14. van Wachem BGM, Schouten JC, Krishna R, van den Bleek CM. Validation of the Eulerian simulated dynamic behavior of gas–solid fluidized beds. *Chem Eng Sci*. 1999;54:2141–2149.
15. Boemer A, Qi H, Renz U. Eulerian simulation of bubble formation at a jet in a two-dimensional fluidized bed. *Int J Multiph Flow*. 1997;23:927–944.
16. Lettieri P, Newton D, Yates JG. Homogeneous bed expansion of FCC catalysts, influence of temperature on the parameters of the Richardson-Zaki equation. *Powder Technol*. 2002;123:221–231.
17. Chu JC, Kalil J, Wetteroth WA. Mass transfer in a fluidized bed. *Chem Eng Progr*. 1953;49:141.
18. Gunn DJ. Transfer of heat or mass to particles in fixed and fluidized beds. *Int J Heat Mass Transf*. 1978;21:467–476.
19. Furusaki S, Nakagiri K, Nozaki Y. Mass transfer coefficients and amounts of direct-contact catalysts in fluidized catalysts beds. *Can J Chem Eng*. 1984;62:610–616.
20. Kai T, Imamura T, Takahashi T. Hydrodynamic influences on mass transfer between bubble and emulsion phases in a fine particle fluidized bed. *Powder Technol*. 1995;83:105–110.
21. Foka M, Chaouki J, Guy C, Klvana D. Gas phase hydrodynamics of a gas-solid turbulent fluidized bed reactor. *Chem Eng Sci*. 1996;51:713–723.
22. Fluent, Inc., *Fluent 6.2: Fluent User's Guide*, 2005.
23. Patankar SV. *Numerical Heat Transfer and Fluid Flow*. Washington DC: Hemisphere Publishing Corporation, 1980.
24. van Wachem BGM, Schouten JC, Krishna R, van den Bleek CM. Eulerian simulations of bubbling behavior in gas-solid fluidized beds. *Comput Chem Eng*. 1998;22:s299–s306.
25. Lun CKK, Savage SB, Jeffrey DJ, Chepurniy N. Kinetic theories for granular flow: inelastic particles in couette flow and slightly inelastic particles in a general flow field. *J Fluid Mech*. 1984;140:223–256.

Appendix

The conservation and constitutive equations used in this article are given below.

Conservation equations

The following are conservation equations of mass, momentum, and species for the gas and particulate phases as well as the particulate phase fluctuating energy.

Mass conservation equations of gas and solid phases. The continuity equation for gas phase, g, is

$$\frac{\partial(\alpha_g\rho_g)}{\partial t}+\frac{\partial}{\partial x_j}(\alpha_g\rho_g u_{gj})=(m_{pg}-m_{gp}) \tag{A1}$$

The continuity equation for particle phase, p, writes

$$\frac{\partial(\alpha_p\rho_p)}{\partial t}+\frac{\partial}{\partial x_j}(\alpha_p\rho_p u_{pj})=(m_{gp}-m_{pg}) \tag{A2}$$

Each computational cell is shared by the interpenetrating phases, so that the sum over all volume fractions is unity,

$$\alpha_p+\alpha_g=1 \tag{A3}$$

Momentum conservation equations of gas and solid phases. The momentum conservation equation for the gas phase, g, is

$$\frac{\partial}{\partial t}(\alpha_g\rho_g u_{gi})+\frac{\partial}{\partial x_j}(\alpha_g\rho_g u_{gi}u_{gj})=-\alpha_g\frac{\partial p}{\partial x_i}+\frac{\partial\tau_{g,ij}}{\partial x_j}-\beta(u_{gi}-u_{pi})+\rho_g\alpha_g g_i+(m_{pg}u_{pi}-m_{gp}u_{gi}) \tag{A4}$$

The momentum conservation equation for the particulate phase, p, can be expressed as

$$\frac{\partial}{\partial t}(\alpha_p\rho_p u_{pi})+\frac{\partial}{\partial x_j}(\alpha_p\rho_p u_{pi}u_{pj})=-\alpha_p\frac{\partial p}{\partial x_i}+\frac{\partial\tau_{p,ij}}{\partial x_j}-\beta(u_{pi}-u_{gi})+\rho_p\alpha_p g_i+(m_{gp}u_{gi}-m_{pg}u_{pi}) \tag{A5}$$

The fluctuations that occur in the particulate phase were modeled from the kinetic theory of gases modified to account for inelastic collisions between particles. The equation for the turbulent fluctuating energy of the particulate phase, p, can then be expressed as

$$\frac{3}{2}\left[\frac{\partial(\alpha_p\rho_p\Theta)}{\partial t}+\frac{\partial(\alpha_p\rho_p u_{pk}\Theta)}{\partial x_k}\right]=\frac{\partial}{\partial x_k}\left(\Gamma_\Theta\frac{\partial\Theta}{\partial x_k}\right)+\mu_p\left(\frac{\partial u_{pk}}{\partial x_i}+\frac{\partial u_{pi}}{\partial x_k}\right)\frac{\partial u_{pk}}{\partial x_i}-p_p\frac{\partial u_{pk}}{\partial x_k}+\left(\xi_p-\frac{2}{3}\mu_p\right)\left(\frac{\partial u_{pk}}{\partial x_k}\right)^2-\gamma \tag{A6}$$

Species conservation equations of gas and solid phase. The species conservation equation for the gas phase, g, is

$$\frac{\partial}{\partial t}(\alpha_g\rho_g Y_{gs})+\frac{\partial}{\partial x_j}(\alpha_g\rho_g Y_{gs}u_{gj})=\frac{\partial}{\partial x_i}\left(\alpha_g\rho_g D_{gs}\frac{\partial Y_{gs}}{\partial x_j}\right)+(m_{psgs}-m_{gsps}) \tag{A7}$$

The species conservation equation for solid phase, p, writes

$$\frac{\partial}{\partial t}(\alpha_p\rho_p Y_{ps})+\frac{\partial}{\partial x_j}(\alpha_p\rho_p Y_{ps}u_{pj})=\frac{\partial}{\partial x_i}\left(\alpha_p\rho_p D_{ps}\frac{\partial Y_{ps}}{\partial x_j}\right)+(m_{gsps}-m_{psgs}) \tag{A8}$$

Constitutive equations

Constitutive relations are needed to close the governing relations. The following are the constitutive relations used in the current model.

The stress tensor for the gas phase,

$$\tau_{g,ij}=\mu_g\left(\frac{\partial u_{gj}}{\partial x_i}+\frac{\partial u_{gi}}{\partial x_j}\right) \tag{A9}$$

The stress tensor of particulate phase,

$$\tau_{p,ij} = \mu_p\left(\frac{\partial u_{pj}}{\partial x_i} + \frac{\partial u_{pi}}{\partial x_j}\right) + \left(\xi_p - \frac{2}{3}\mu_p\right)\frac{\partial u_{pk}}{\partial x_k}\delta_{ij} - p_p\delta_{ij} \tag{A10}$$

The particulate pressure (p_p) is composed of two parts: a kinetic term that dominates in the dilute flow regions and a collision contribution that is significant in the dense flow regions,

$$p_p = \alpha_p\rho_p[1 + 2(1+e)\alpha_p g_0]\Theta \tag{A11}$$

where, e is the restitution coefficient. The radial distribution function, g_0, is a correction factor that modifies the probability of collisions between grains when the granular phase becomes dense, is expressed as,

$$g_0 = \left[1 - \left(\frac{\alpha_p}{\alpha_{p,max}}\right)^{1/3}\right]^{-1} \tag{A12}$$

Θ is granular temperature, defined by,

$$\Theta = \frac{1}{3}\left\langle \overline{u'_p u'_p} \right\rangle \tag{A13}$$

Solids phase shear viscosity,

$$\mu_p = \frac{2\mu_{p,dil}}{(1+e)g_0}\left[1 + \frac{4}{5}(1+e)g_0\alpha_p\right]^2 + \frac{4}{5}\alpha_p^2\rho_p d_p g_0(1+e)\sqrt{\frac{\Theta}{\pi}} \tag{A14}$$

Solids phase dilute viscosity,

$$\mu_{p,dil} = \frac{5}{96}\rho_p d_p\sqrt{\pi\Theta} \tag{A15}$$

The solids bulk viscosity accounts for the resistance of the granular particles to compression and expansion. It has the following form,

$$\xi_p = \frac{4}{3}\alpha_p^2\rho_p d_p g_0(1+e)\sqrt{\frac{\Theta}{\pi}} \tag{A16}$$

The diffusion coefficient for the solid phase energy fluctuation is,

$$\Gamma_\Theta = \frac{2\Gamma_{\theta,dil}}{(1+e)g_0}\left[1 + \frac{6}{5}(1+e)g_0\alpha_p\right]^2 + 2\alpha_p^2\rho_p d_p g_0(1+e)\sqrt{\frac{\Theta}{\pi}} \tag{A17}$$

$$\Gamma_{\Theta,dil} = \frac{75}{384}\rho_p d_p\sqrt{\pi\Theta} \tag{A18}$$

The collisional dissipation of energy fluctuation is,

$$\gamma = 3(1-e^2)\alpha_p^2\rho_p g_0\Theta\left[\frac{4}{d_p}\sqrt{\frac{\Theta}{\pi}} - \frac{\partial u_{pk}}{\partial x_k}\right] \tag{A19}$$

Manuscript received Apr. 20, 2007, and revision received Jan. 5, 2008.